Parametric modelling of the performance of a 5-kW proton-exchange membrane fuel cell stack

J.C. Amphlett, R.M. Baumert, R.F. Mann, B.A. Peppley, P.R. Roberge and A. Rodrigues

Department of Chemistry and Chemical Engineering, Royal Military College of Canada, Kingston, Ont., K7K 5L0 (Canada)

Abstract

A parametric model predicting the performance of a solid polymer electrolyte, proton-exchange membrane fuel cell has been developed using a combination of mechanistic and empirical modelling techniques. Mass-transport properties, thermodynamic equilibrium potentials, activation overvoltages, and internal resistance were defined by fundamental relations. But the mechanistic model, however, could not completely model fuel cell performance, since several simplifying approximations had been used to facilitate model development. Additionally, certain properties likely to be observed in operational fuel cells, such as thermal gradients, have not been considered. Nonetheless, the insights gained from the mechanistic assessment of fuel cell processes were found to give the resulting empirical model a firmer theoretical basis than many of the models presently available in the literature. Correlation of the empirical model to actual experimental data was very good. The performance of a Ballard Mark V 35-cell stack, using a Nafion™ electrolyte membrane, and operating on inlet feeds of air (150% excess) and hydrogen (15% excess) has been modelled parametrically, based on a model previously developed for a Ballard Mark IV single cell.

Introduction

A model mapping overvoltages in a proton-exchange membrane (PEM) fuel cell as a function of various contributing variables can be of great utility to researchers and operators. Two common fuel cell modelling approaches are: (i) mechanistic modelling and (ii) empirical analysis. Although, many mechanistic models can be found in the literature [1–4], they generally require the knowledge of parameters not readily available such as transfer coefficients, internal humidity levels, membrane, electrode, and active catalyst layer thicknesses. Empirical models [5–7], on the other hand, are generally only accurate over a small operating range. They fail to reflect the actual processes involved in fuel cell operation and, thus, are not applicable over a broad range of conditions. An approach combining both mechanistic and empirical modelling has the potential to couple both mechanistic validity and the inherent simplicity of the empirical approach.

In this paper, the performance of a Ballard Mark V 35-cell stack, using a Nafion™ electrolyte membrane, and operating on inlet feeds of air and hydrogen has been modelled parametrically, based on a model previously developed [6, 8] for a Ballard Mark IV single cell. A three-stage approach was followed. Initially, mechanistic modelling techniques were employed to determine the characteristic dependencies of fuel cell

SSDI 0378-7753(93)01835-6

operation. This yielded simple algebraic expressions defining the thermodynamic equilibrium potential, as well as overvoltages due to activation, ohmic resistance and mass-transport properties.

In the second stage, numerical parametric equations for each of the voltage losses were determined from experimental data. These equations reflected the form of the algebraic expressions developed in the first stage. The final stage involved the statistical analysis of the resulting parametric model. The output voltage (V) of each cell was defined with eqn. (1) as a function of the thermodynamic equilibrium potential (E) corresponding to the overall chemical reaction expressed in eqn. (2), the activation overvoltage (η_{act}) and the ohmic overvoltage (η_{ir}).

$$V = E + \eta_{act} + \eta_{ir} \tag{1}$$

$$2H_{2(g)} + O_{2(g)} = 2H_2O_{(aq)} \tag{2}$$

The thermodynamic potential was defined in terms of the input variables with eqns. (3) and (4) where T is the temperature (K), i the current (A), n the number of participating electrons, F is Faraday constant, $p^*_{O_2}$ and $p^*_{H_2}$ are, respectively, the effective partial pressures of oxygen (eqn. (5)) and hydrogen (eqn. (6)), E°_0 the standard state reference potential (equal to 1.229 V at 298.15 K and 1 atm) and ΔS° the entropy change of reaction (eqn. (2)):

$$E = E^\circ - \frac{RT}{nF}\left[\ln(p^*_{O_2}) + 2\ln(p^*_{H_2})\right] \tag{3}$$

$$E^\circ = E^\circ_0 + (T - 298.15)\left(\frac{\Delta S^\circ}{nF}\right) \tag{4}$$

$$p^*_{O_2} = p_{air}\exp\left(-\frac{RTil_d}{4FpD^{eff}_{H_2O,\,O_2}}\right) - p_{sat} \tag{5}$$

$$p^*_{H_2} = 0.5p^*_{H_2}\exp\left(-\frac{RTil_d}{4FpD^{eff}_{H_2O,\,H_2}}\right) - p_{sat} \tag{6}$$

In eqns. (5) and (6), the variables $p^*_{O_2}$ and $p^*_{H_2}$ are defined in terms of their controlled equivalent p_{air} and p_{H_2}. In these expressions, the pressure diffusivity product, $pD^{eff}_{H_2O,\,H_2}$, and the thickness of the gas diffuser portion of the electrode, l_d, were estimated from ref. 4.

Experimental

The initial fuel cell model [6, 8] was developed for the data gathered with a single cell of the Mark IV design produced by Ballard Power Systems Inc., North Vancouver, BC. The cell consisted of a sandwich of DuPont's Nafion 117™ membrane between two carbon fibre paper electrodes with the face of each electrode contacting the membrane impregnated with platinum catalyst and Teflon. The geometric surface area of the Mark IV cell was 50.6 cm^2.

The test model was then extended to a Ballard Mark V 5-kW system, also known as a Globe 90 unit, which consisted of a 35 PEM fuel cell stack integrated with automatic processing and control support systems. Each cell of the stack had an active area of 230 cm^2 and operated with a Nafion 117™ membrane and a platinum catalyst.

In order to extend its experimental testing capabilities, the system was modified by enhancing its temperature control and by adding gas flow and temperature monitoring. In order to facilitate an expanded experimental range, Ballard's cell voltage comparator (CVC) was also reprogrammed to allow for wider variation between cell group voltages. A schematic representation of the Globe 90 testing system is presented in Fig. 1. The range for each controlled variable used during the testing of the Globe 90 unit is given in Table 1.

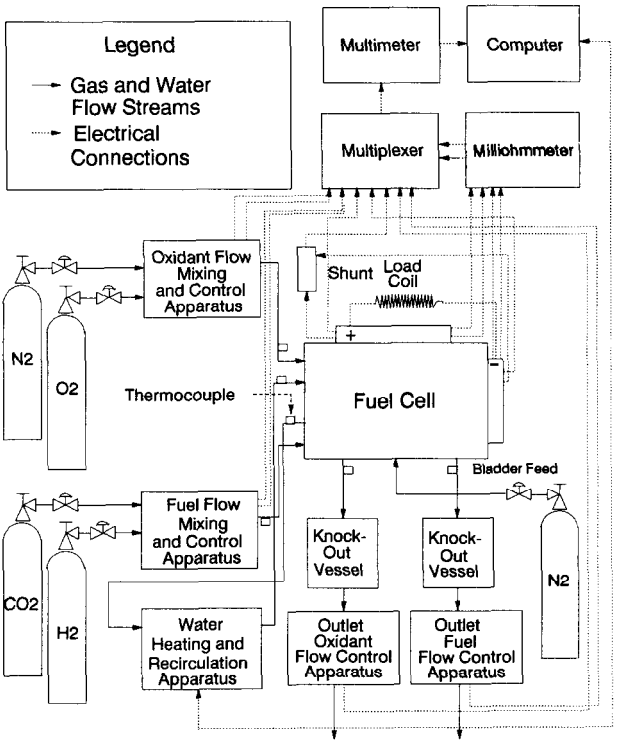

Fig. 1. Schematic of the re-engineered Globe 90 fuel cell system.

TABLE 1

Ranges of the controlled variables used in the experimental design of the tests performed on the Globe 90 fuel cell unit

Test no.	SR[a]	T (K)		i (A)		Inlet p_{air} (kPa)		Inlet p_{H_2} (kPa)	
		min	max	min	max	min	max	min	max
1	1.15/2.5	333	353	32	125	275	375	275	375
2	2.0/2.0	333	350	34	100	175	455	310 (constant)	

[a]Stoichiometric ratio or ratio of the inlet oxygen flow rate to the rate at which it is consumed.

The mechanistic model

The envisaged electrode structure comprises two regions: (i) a porous, partially hydrophobic, carbon fibre-paper backing layer, and (ii) a very thin, hydrophobic layer of platinum catalyst and Teflon binder lying between the electrode and the membrane. Of this second layer, only the uppermost catalyst agglomerates (5 nm < radius < 50 nm) are believed to directly contact the membrane phase [1, 2]. It is assumed that the walls of the macropores between carbon fibres are coated with hydrophobic Teflon, while the walls of the micropore within carbon fibres will not be Teflon coated. The wet-proofed macropores provide a path for gas flow in the cathode, while the micropores provide a path for liquid product water to exit the flow channels. A similar approach to water and gas transport in the electrode has been previously suggested by Verbrugge and Bernardi [3].

The hydrophobic nature of the Teflon binder is expected to cause the product water to bead. This will repel the resulting liquid microdroplets out of the catalyst layer and into the non-hydrophobic micropores of the carbon fibre-paper backing, through which they will flow to the gas flow channels. Here they will be entrained in the gas flow and removed from the fuel cell. While the Teflon is expected to be very effective in removing product water from the catalyst layer, the agglomerate theory of Ridge *et al.* [2] suggests that a microfilm of water will still coat the catalyst particles.

Considering the proposed physical characteristics, the expected transport processes at the cathode are: (i) diffusion of humidified oxygen (with a possible nitrogen fraction) through the wet-proofed pores of the porous backing layer; (ii) diffusion of dissolved oxygen through a water film in the catalyst layer, and (iii) capillary and surface tension induced flow of water microdroplets through non-wet-proofed pores in the carbon fibre backing layer. It is is assumed that the non-wet-proofed pores are closed to gas flow at all current densities, such that the effective porosity of the cathode (in terms of gas flow) is constant. The assumption of a constant effective porosity has been employed in all of the mechanistic models reviewed thus far [1–4]. The main assumptions made during the development of the fuel cell model are briefly described in the following list:

- The anode and cathode gases are saturated with water vapour in a humidifier, prior to entry into the flow channels of the cell
- It is expected that a gradient of water concentration will exist across the electrolyte membrane, with the level of hydration increasing from the anode to the cathode. This is expected to lead to diffusion of water from the cathode to the anode
- Three distinct mass-transport interfaces exist in both electrodes: (i) between the gas flow channels and the porous electrodes; (ii) between the gas phase in the electrodes and any water film which may cover the catalyst sites, and (ii) between the water film and the catalyst surface
- The reactant partial pressure in the inlet flow channels will vary with both the humidification level of the inlet streams and the consumption rates of oxygen and hydrogen
- The outlet dry gas composition at the cathode can be calculated as a function of the dry inlet mole fractions, the total pressure and the oxygen stoichiometric ratio (SR is the ratio of the inlet oxygen flow rate to the rate at which it is consumed)
- The diffusivity and concentration of protons as well as the convective proton velocity will all be dependent upon the water content and distribution in the membrane, which is itself dependent on operating current and temperature

TABLE 2

Experimental data obtained from the Mark V fuel cell system for 1.15/2.5 stoichiometry for H_2/air feeds

Run no.	T (K)	Current (A)	$p_{\text{inlet, air}}$ (kPa)	$p_{\text{inlet, H2}}$ (kPa)	Total output voltage (V)	Total R_{int} (mΩ)
1	334	41.0	277	276	27.44	2.99
2	354	31.8	271	270	28.36	2.47
3	333	40.7	324	276	27.45	2.92
4	333	40.9	321	275	27.55	2.85
5	333	124.7	273	273	21.09	3.46
6	353	94.6	270	269	24.32	2.96
7	336	125.3	252	377	24.95	3.68
8	353	95.2	325	277	24.82	2.84
9	334	39.9	274	274	27.44	3.03
10	353	32.3	267	324	28.22	2.55
11	329	39.3	278	379	27.30	3.02
12	353	32.1	322	323	27.75	2.65
13	334	125.4	275	382	20.99	3.46
14	353	94.1	271	325	23.39	3.34
15	333	125.3	376	379	21.74	3.55
16	353	94.9	324	319	24.93	2.67
17	333	39.5	379	377	28.01	2.84
18	333	39.8	377	278	26.62	2.98
19	353	32.0	325	273	28.47	2.51

These assumptions were transformed into practical parametric expressions of η_{act} and η_{ir} through respectively eqns. (7) and (8):

$$\eta_{\text{ac}} = \xi_1 + \xi_2 T + \xi_3 T(\ln i) + \xi_4 T(\ln C^*_{O_2}) \tag{7}$$

$$\eta_{\text{ir}} = iR_{\text{int}} = i(\xi_5 + \xi_6 T + \xi_7 i) \tag{8}$$

In these equations, the ξs represent constant parametric coefficients, R_{int} is the internal resistance and $C^*_{O_2}$ is the effective oxygen concentration (mol/cm^3) at the cathode, which is defined in terms of $p^*_{O_2}$ with Henry's law expression in eqn. (9):

$$C^*_{O_2} = p^*_{O_2} \times 1.97 \times 10^5 \exp\left(\frac{498}{T}\right) \tag{9}$$

Results and discussion

With the experimental apparatus configured to monitor all of the necessary variables, a three-level experimental design using 28 runs was employed to generate the data required for the linear regression analysis. The independent variables controlled in the experiment were the fuel cell temperature, the operating current, and the inlet partial pressures of hydrogen and oxygen. The dependent variables monitored included the output voltage (V) and the total resistance (internal and load resistance in parallel). Given the acquired data, separation of the monitored resistance into internal and load

TABLE 3

Experimental data obtained from the Mark V fuel cell system for 2.0/2.0 stoichiometry for H_2/air feeds

Run no.	T (K)	Current (A)	$p_{\text{inlet air}}$ (kPa)	$p_{\text{inlet, H2}}$ (kPa)	Total output voltage (V)	Total R_{int} (mΩ)
1	278	36.9	402	310	28.65	2.53
2	333	36.9	198	310	27.20	2.91
3	341	34.4	241	311	28.08	2.71
4	334	58.4	174	313	25.16	3.19
5	334	59.5	232	308	25.94	3.00
6	335	97.1	228	311	22.86	3.18
7	341	90.8	349	310	25.01	2.87
8	341	35.9	318	307	28.19	2.68
9	341	90.5	260	312	23.49	2.93
10	347	51.3	353	311	27.54	2.86
11	348	52.7	451	306	27.97	2.95
12	349	79.1	406	310	25.98	2.63
13	341	55.4	285	307	26.60	2.65
14	341	55.6	285	309	26.73	2.67
15	341	55.5	287	308	26.68	2.60

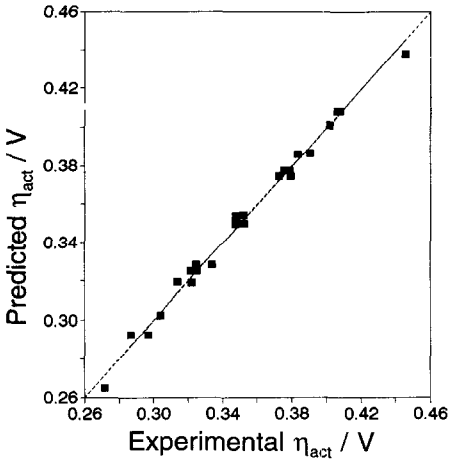

Fig. 2. Parity plot of the model prediction and the experimental data for the activation overvoltage of a Ballard Mark V PEM fuel cell.

components allowed for the determination of the actual ohmic overvoltage via eqn. (8).

Tables 2 and 3 contain the experimental data obtained by operating the Mark V in the two sets of test conditions described in Table 1. Voltage and resistance were monitored across each cell of the 35-cell stack. Results for the 5 highest and 5 lowest values were discarded and the average voltage and resistance of the 25 remaining cells were modelled. The parametric coefficients (ξ) contained in

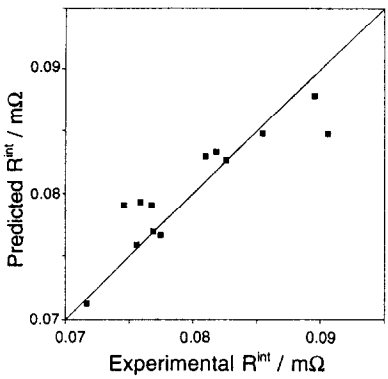

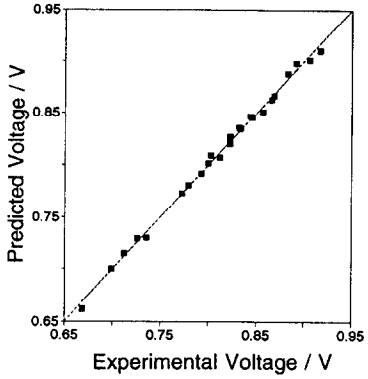

Fig. 3. Parity plot of the model prediction and the experimental data for the internal resistance of a Ballard Mark V PEM fuel cell.

Fig. 4. Parity plot of the model prediction and the experimental data for the total output voltage of a Ballard Mark V PEM fuel cell.

eqns. (7) and (8) were then derived from the linear regression of the experimental data. The results of this analysis are presented in the following list:

$\xi_1 = -0.694$
$\xi_2 = 4.34 \times 10^{-3}$
$\xi_3 = -1.96 \times 10^{-4}$
$\xi_4 = 1.80 \times 10^{-5}$
$\xi_5 = 3.30$
$\xi_6 = -7.55 \times 10^{-3}$
$\xi_7 = 1.10 \times 10^{-3}$

By substituting these experimental coefficients in eqns. (7) and (8) and using the global eqn. (1), it was possible to arrive at a model of the voltage behaviour of the Mark V cell stack. The quality of the fit of this model to the experimental results is illustrated in the parity plots of modelled versus experimental values for activation overvoltage, ohmic resistance and voltage output presented respectively in Figs. 3 and 4.

Conclusions

Predictions of the resulting model showed very good agreement with actual cell performance for the majority of cells in the 35-cell stack. Deviations from predicted values were observed most commonly in the cell groups closest to the ends of the stack, indicating the possibility of water and gas flow variations within the flow manifold. Very good agreement between the empirical model and the experimental data indicates the value of developing a mechanistic basis for empirical modelling exercises. This approach is of considerable benefit in expanding the applicability and validity of the empirical model produced. In spite of the assumptions and approximations employed in the mechanistic approach, the predictions of the model appear to reflect the actual trends found in the experimental data. As a result of its mechanistic basis, the empirical model can be extrapolated beyond the experimental range with much more confidence

than would otherwise be justified. Yet, its application maintains the ease and empirical validity for which empirical models are known. The effort, involved in coupling mechanistic and empirical approaches to model the performance of a PEM fuel cell, was found to be worthwhile and the final model to be both mechanistically valid and friendly to use.

References

1 R.P. Iczkowski and M.B. Cutlip, *J. Electrochem. Soc., 127* (1980) 1433.
2 S.J. Ridge, R.E. White, Y. Tsou, R.N. Beaver and G.A. Eisman, *J. Electrochem. Soc., 136* (1989) 1902.
3 M.W. Verbrugge and D.M. Bernardi, *AIChE J., 37* (1991) 1151.
4 T.E. Springer, T.A. Zawodzinski and S. Gottesfeld, *J. Electrochem. Soc., 138* (1991) 2334.
5 H. Ide, T. Yoshida, H. Ueda and N. Horiuchi, *Proc. 24th Intersociety Energy Conversion Conf., Washington, DC, USA, 1989,* pp. 1517–1522.
6 J.C. Amphlett, M. Farahani, R.F. Mann, B.A. Peppley and P.R. Roberge, *Proc. 26th Intersociety Energy Conversion Conf., Boston, MA, USA, 1991,* pp. 624–630.
7 A. Cisar, *Proc. 26th Intersociety Energy Conversion Conf., Boston, MA, USA, 1991,* pp. 611–616.
8 J.C. Amphlett, R. Baumert, T.J. Harris, R.F. Mann, B.A. Peppley and P.R. Roberge, *J. Electrochem. Soc.,* in press.